

**18th International Conference on
Harmonisation within Atmospheric Dispersion Modelling for Regulatory Purposes
9-12 October 2017, Bologna, Italy**

VALIDATION METRICS FOR TIME DEPENDENT OBSTACLE RESOLVING SIMULATIONS

Jörg Franke¹ and Thanh H. Pham¹

¹Faculty of Engineering, Vietnamese-German University, Thu Dau Mot, Vietnam

Abstract: The increase of turbulence resolving time-dependent simulations for dispersion makes thorough validation of these approaches more urgent, comparing more data than only low order statistics like mean values and variances. The quantitative comparison of more complex data requires mostly different metrics from those used for low order statistics. In this contribution, we suggest a metric based on cumulative distribution functions for the quantitative comparison of frequency distributions, which was originally proposed for validation of probabilistic predictions in the context of model-form uncertainty. The metric is applied to horizontal wind direction fluctuations in boundary layer flow in an empty wind tunnel, with simulation data obtained by Large Eddy Simulation. In addition the corresponding low order statistics are compared qualitatively and quantitatively to provide a comprehensive overview of the simulation result.

Key words: *Validation metrics, large eddy simulation, precursor simulation, Michelstadt.*

INTRODUCTION

The increase of time-dependent simulations for dispersion, like for example Large Eddy Simulation (LES) and Detached Eddy Simulation (DES) makes thorough validation of these approaches more urgent. Hertwig et al. (2017a) recently stated that most validations of time-dependent simulations to date did only focus on low order statistics, not making use of the rich information in the time-dependent data. They proposed a multi-level approach for validation, from global statistics over eddy statistics to scale statistics, and exemplified it for wind tunnel and LES investigations of the flow in the inner city of Hamburg (Hertwig et al., 2017b). While they used standard metrics for the quantitative comparison of low order statistics (e.g. Hanna and Chang, 2012), they only graphically compared the many other data that they extracted, including frequency distributions of horizontal wind direction fluctuations, which clearly shows the need to discuss metrics for eddy and scale statistics.

Ferson et al. (2008) suggested a metric for validation of probabilistic predictions which is based on cumulative distribution functions (CDFs) from experiment and numerical simulation. This metric will be introduced in the following and applied to the comparison of measured and simulated horizontal wind direction fluctuations in boundary layer flow in an empty wind tunnel. The LES was done as precursor simulation to generate time-dependent inflow boundary conditions for subsequent simulations of the Michelstadt case (Hertwig et al., 2012; Rakai and Franke, 2014) to conduct rigorous validation of LES for urban flow and dispersion. The experimental data are taken from the case BL3-0-0 within the CEDVAL-LES database (Fischer et al., 2010).

To provide comprehensive information on the investigated case, the authors decided to use this extended abstract to present the computational setup, which differs significantly from the one described by Franke and Pham (2017), in sufficient detail, as well as the exploratory data analysis and hit rate as well-known metric for the lower order statistics, and the definition of the so called area metric of Ferson et al. (2008) together with results from its application to wind direction statistics. The detailed discussion of these results and provision of further information like spectra and time scales will be provided in the presentation slides.

SIMULATION PARAMETERS

The computational domain of the empty wind tunnel with vortex generators and roughness elements is shown in Figure 1. The length and width of the domain are 15.85 m and 4 m, respectively, the height varies between 2.57 and 2.62 m in x -direction to minimize the streamwise pressure gradient. The vortex generators are distributed symmetrically over the domain width and 35 rows of roughness elements with two sizes of $0.04 \times 0.04 \text{ m}^2$ and $0.08 \times 0.08 \text{ m}^2$ are reproduced. Vortex generators and roughness elements are modelled as zero thickness surfaces. The roughness elements are grouped in a repeating pattern of four rows, where one row is composed of only small elements and one row of only large elements while the other two rows consist of alternating elements (Bastigkeit, 2011; Franke and Pham, 2017).

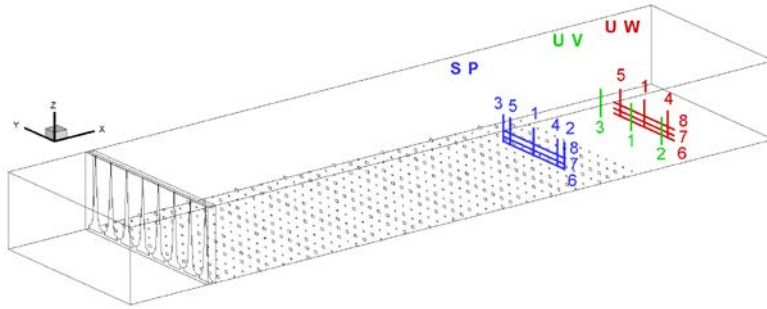


Figure 1. Computational domain with vortex generators, roughness elements and data locations (blue: sampling plane SP, green: UV measurements, red: UW measurements)

In the numerical simulation only those roughness elements also used in the experiments with the Michelstadt model in the wind tunnel are included in the computational domain, while for the experiments in the empty wind tunnel the entire floor was covered by roughness elements. The experimental velocity measurement locations named UV and UW in Figure 1 were therefore within the roughness elements in the experiments while they are located in the region with smooth floor in the numerical simulation. Only the locations within the sampling plane for inflow velocity conditions, named SP in Figure 1, are located within the roughness elements in the numerical simulation.

The computational domain was meshed with a hybrid grid of approximately ten million cells. The region around the vortex generators was meshed unstructured with tetrahedral cells, while the rest of the domain was meshed block-structured with hexahedral cells. Pyramids were used between tetrahedral and hexahedral cells to generate a conformal grid throughout the entire computational domain. Wall adjacent cells are relatively coarse with 0.02 m height.

LES of the flow was performed with OpenFOAM 2.4.0 by solving the implicitly filtered Navier-Stokes equations with constant density and viscosity. Subgrid scales were modelled with the dynamic one-equation model for the subgrid scale kinetic energy. The local filter width was computed as cubic root of the cell volumes and a top-hat was used as test filter in the dynamic procedure. Due to the coarse wall adjacent grid the Spalding wall function was used at all wall boundaries. At the inflow plane a constant velocity of 5 ms^{-1} in x -direction was prescribed and the static pressure fixed at the outlet.

Numerical approximations are the 2nd order backward scheme for time derivatives and the 2nd order central differencing with explicit non-orthogonal corrections for the diffusive terms. Convective terms in the momentum and subgrid scale kinetic energy equations were approximated by the 2nd order linear upwind scheme with SUPERBEE limiter. Finally, 2nd order differencing with multi-dimensional cell limiter was used for the gradient of the resolved pressure. The algebraic equations were solved by *pisoFoam* with constant time step size of 0.001 s, yielding maximum Courant numbers of up to seven within each time step. Convergence per time step was reached when the iterative tolerance dropped below 10^{-6} . The startup phase of the simulation lasted for 10 s, corresponding to approximately three flow through times. Data sampling was then performed for 120 s, approximately 38 flow through times, with data recorded at every fourth time step yielding a sampling rate of 250 Hz.

RESULTS

Velocity measurements were done by 2D Laser Doppler Anemometry. Therefore only two velocity components are available at each measurement location. This is reflected in the naming of the profiles in Figure 1. At UV profiles only streamwise U and lateral V were measured, and at UW profiles streamwise U and vertical W. Corresponding coordinates are x, y and z in streamwise, lateral and vertical direction, with $z = 0$ m defining the bottom wall of the wind tunnel.

Experimental velocity data were sampled for longer durations between 200 s and about 300 s with varying sampling rates. For the Discrete Fourier Transformation to analyse power spectral densities and for the temporal autocorrelation to analyse integral time scales (not shown in this contribution), the experimental time series were resampled with constant sampling rate. Resampling was done by cubic Hermite spline interpolation respecting the minima and maxima of the original time series.

For the computation of lower order statistics the full experimental time series were segmented into time series of 120 s lengths with 90% overlap. Lower order statistics were then calculated for the individual 120 s segments and subsequently averaged over the number of segments to yield the mean experimental values and their 95% confidence intervals presented in the next section.

All simulation data are made non-dimensional with the mean streamwise velocity at location $(x,y,z) = (0,0,0.44)$ m taken as reference velocity U_{ref} . The experimental reference velocity was taken at the same height, but the (x,y) location is unknown.

Lower order statistics

The non-dimensional mean streamwise velocity component at the profiles in the wind tunnel centre (numbers 1 in Figure 1) are shown in Figure 2a). The velocity agrees very well with the measurements down to a height of $z \approx 0.2$ m, corresponding to 2.5 times the height of the large roughness elements. Below the simulation results at location UV1 and UW1 are higher than the experiments due to the smooth wall in the simulations. The simulation result at SP1 agrees however very well with the experiment at location UV1, which has the same relative location within the four repeating rows of the roughness array. At measurement location UW1 velocities are smaller close to the ground due to the influence of a small roughness element located upstream.

The agreement between the lateral velocity components predicted at SP1 and UV1 with the experimental data at UV1 is also very good, although the absolute values are very small, see Figure 2b). Larger discrepancies exist for the vertical velocity component where only close to the ground the simulation at SP1 and measurement at UW1 is close, see Figure 2c).

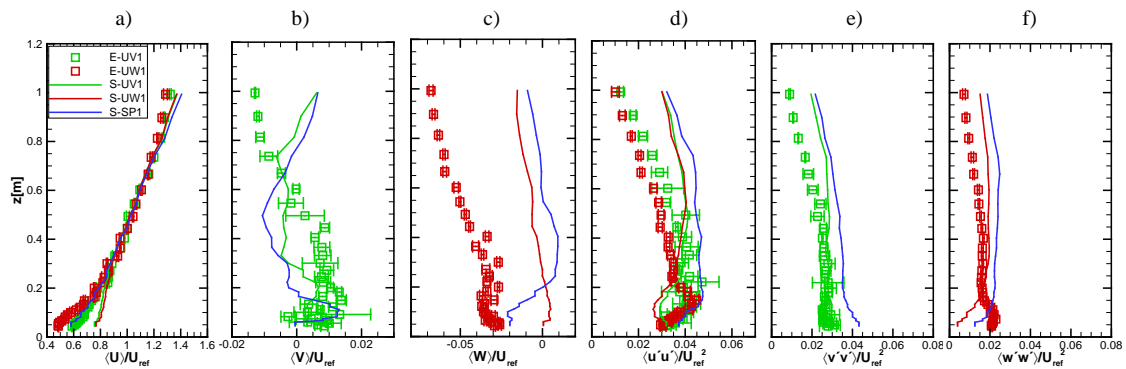


Figure 2. Non-dimensional mean velocities and normal Reynolds stresses at profiles located in the centre.

Also for the non-dimensional normal components of the Reynolds stress tensor the agreement is good. In streamwise direction, Figure 2d), the simulation results SP1 agree very well with the experiments at UV1 and UW1 up to $z \approx 0.2$ m, while above the simulation renders higher values, most likely due to the shorter distance to the vortex generators. The simulation results at UV1 and UW1 are lower than the experiments close to the bottom wall and agree better with the experiments than the results of SP1 at larger heights.

Similar results are obtained for the vertical normal Reynolds stress, Figure 2f), where the difference between the simulation result at SP1 and the measurement at UW1 close to the bottom wall might be attributed to the influence of the upstream roughness element in the experiment. Finally, the lateral normal Reynolds stress is overpredicted by the simulation at SP1 but very well captured by the simulation results at UV1.

For the quantitative comparison of simulation and experiment the hit rate (Schatzmann et al., 2010) is used as metric for the lower order statistics with 0.25 for the allowed relative difference and the local 95% confidence intervals for the allowed absolute difference. The hit rate is evaluated for all profiles shown in Figure 1, consisting of 96 locations for UV and 153 locations for UW. Two values for the hit rates are provided for UV and UW, one for the comparison of results at the same location, e.g. UV - UV, and one for the comparison between experiments and simulation results at SP at the corresponding locations, e.g. SP - UV. The hit rates are presented in Table 1.

Table 1. Hit rates for non-dimensional mean velocities and Reynolds stresses

Profiles	$\langle U \rangle / U_{\text{ref}}$	$\langle V \rangle / U_{\text{ref}}$	$\langle W \rangle / U_{\text{ref}}$	$\langle u'u' \rangle / U_{\text{ref}}^2$	$\langle v'v' \rangle / U_{\text{ref}}^2$	$\langle w'w' \rangle / U_{\text{ref}}^2$	$\langle u'v' \rangle / U_{\text{ref}}^2$	$\langle u'w' \rangle / U_{\text{ref}}^2$
SP - UV	1.00	0.12	-	0.75	0.35	-	0.42	-
SP - UW	1.00	-	0.08	0.60	-	0.34	-	0.31
UV - UV	0.79	0.10	-	0.70	0.62	-	0.31	-
UW - UW	0.63	-	0.00	0.67	-	0.54	-	0.29

As expected from the graphical comparison in Figure 2, hit rates for the streamwise velocity component are high, reaching even 1 when comparing results at SP with the measurement locations UV and UW. The hit rates for the other velocity components are much lower, for the vertical velocity component even 0 when data at UW are compared. With the exception of the lateral normal component, the Reynolds stresses show the same behaviour with higher hit rates for the comparison with SP simulation data.

Horizontal wind direction fluctuation frequency distribution

Comparison of frequency distributions of wind direction is another important method to compare experiments with numerical simulations (Hertwig et al., 2017a). Here the instantaneous horizontal wind direction fluctuation around the mean direction is denoted by the angle θ and defined as

$$\theta = \tan^{-1}(V/U) - \overline{\tan^{-1}(V/U)}, \quad (1)$$

where U and V are instantaneous velocity components and the overbar denotes a time average over the entire time series. Frequency distributions of θ are shown in Figure 3a) at four different heights. Both experiment and simulation show a narrowing of the distributions with increasing height, corresponding to the transition from small scale turbulent structures to larger scale turbulent structures when moving away from the bottom wall.

In Figure 3b) the corresponding CDFs of θ are depicted in the relevant range. This presentation still shows the much narrower distribution of the fluctuations at the lowest point, but does no longer reveal the differences in the peak values as the frequency distribution in Figure 3a).

To quantitatively compare CDFs, Ferson et al. (2008) proposed for validation of probabilistic predictions the so called area metric AM, defined as

$$AM_{\theta} = \int_{-\infty}^{\infty} |CDF_S(\theta) - CDF_E(\theta)| d\theta, \quad (2)$$

where index S refers to simulation and index E to experiment. This metric corresponds to the area between the distributions of the simulation and of the experiment, retaining the units of the variable of interest. A detailed discussion on the pros and cons of this metric can be found in Ferson et al. (2008).

The metric was applied to all locations on profile UV1 see Figure 3c). Highest differences between simulation and experiment are again found close to the bottom and decrease with height.

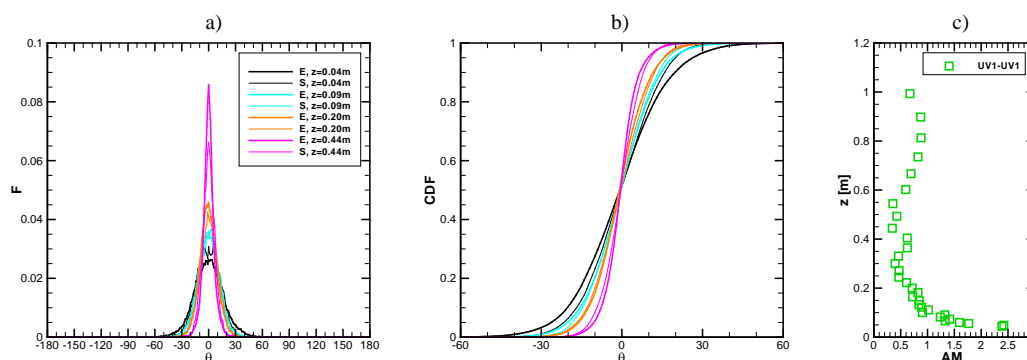


Figure 3. Horizontal wind direction fluctuations, a) frequency distributions, b) CDFs, c) area metrics at UV1

CONCLUSION

LES of a boundary layer flow in an empty wind tunnel was validated against corresponding experiments. Low order statistics agree with high hit rates for the streamwise velocity and normal Reynolds stress component, while lateral and vertical velocity component are poorly predicted, and the other Reynolds stress components are satisfactorily determined. For the CDF of horizontal velocity fluctuations the area metric of Ferson et al. (2008) is used, yielding results that are consistent with the lower order statistics. A more detailed discussion of this metric will be provided in the presentation together with results for energy density spectra and integral time scales, extending the analysis to eddy statistics in the flow.

ACKNOWLEDGEMENT

Computing time for the simulation has been generously provided on the High Performance Computing cluster of the Faculty of Computer Science & Engineering, Ho Chi Minh University of Technology, Ho Chi Minh City, Vietnam.

REFERENCES

- Bastigkeit, I., 2011: Erzeugung von Validierungsdaten für wirbelaflösende mikroskalige Strömungs- und Ausbreitungsmodelle, PhD Dissertation, University of Hamburg, Germany, 155 pp.
- Ferson, S., W.L. Oberkampf and L. Ginzburg, 2008: Model validation and predictive capability for the thermal challenge problem. *Computer Methods in Applied Mechanics and Engineering*, 197, 2408–2430.
- Fischer, R., I. Bastigkeit, B. Leitl and M. Schatzmann, 2010: Generation of spatio-temporally high resolved datasets for the validation of LES-models simulating flow and dispersion phenomena within the lower atmospheric boundary layer. In: 5th International Symposium on Computational Wind Engineering, North Carolina, USA.
- Franke, J. and T.H. Pham, 2017: Precursor simulation for LES validation study of the Michelstadt case. In: Proceedings of the 7th European-African Conference on Wind Engineering, Liège, Belgium.
- Hanna, S.R. and J.C. Chang, 2012: Acceptance criteria for urban dispersion model evaluation. *Meteorology and Atmospheric Physics*, **116**, 133-146.
- Hertwig, D., G.C. Efthimiou, J.G. Bartzis and B. Leitl, 2012: CFD-RANS model validation of turbulent flow in a semi-idealized urban canopy. *Journal of Wind Engineering and Industrial Aerodynamics*, **111**, 61-72.
- Hertwig, D., G. Patnaik and B. Leitl, 2017a: LES validation of urban flow, part I: flow statistics and frequency distributions. *Environmental Fluid Mechanics*, **17**, 521-550.
- Hertwig, D., G. Patnaik and B. Leitl, 2017b: LES validation of urban flow, part II: eddy statistics and flow structures. *Environmental Fluid Mechanics*, **17**, 551-578.
- Rakai, A. and J. Franke, 2014: Validation of two RANS solvers with flow data of the flat roof Michelstadt case. *Urban Climate*, **10**, 758-768.
- Schatzmann, M., H. Olesen and J. Franke, 2010: COST 732 Model Evaluation Case Studies: Approach and Results. COST Office, Belgium, 121 pp.